Molecular Dynamics Simulation of Micellar Shape Transition in Amphiphilic Solutions*)

Susumu FUJIWARA, Masato HASHIMOTO, Yuichi TAMURA[1)], Hiroaki NAKAMURA[2)] and Ritoku HORIUCHI[2)]

Kyoto Institute of Technology, Matsugasaki, Sakyo-ku, Kyoto 606-8585, Japan
[1)]*Konan University, 8-9-1 Okamoto, Higashinada-ku, Kobe 658-8501, Japan*
[2)]*National Institute for Fusion Science, 322-6 Oroshi-cho, Toki 509-5292, Japan*

The micellar shape transition in amphiphilic solutions is studied by coarse-grained molecular dynamics simulations of rigid amphiphilic molecules with explicit solvent molecules. Our simulations show that the dominant micellar shape changes from disc to cylinder, and then to sphere as the hydrophilic interaction increases. We find that, as the hydrophilic interaction increases, the potential energy decreases monotonically even during the micellar shape transition, whereas the slope of the potential energy decreases in a stepwise manner in relation to the micellar shape transition. We also ascertained that there exists a wide coexistence region in the intensity of the hydrophilic interaction between a cylinder and a sphere, whereas the coexistence region between a cylinder and a disc is very narrow.

1. Introduction

The spontaneous formation of structures (or self-organization) has been intensively studied in plasmas in order to improve plasma confinement. Such creation of order is universal in nonequilibrium and nonlinear systems interacting with their environment. To explore the universal self-organizing properties in nature, we investigate the structure formation in soft matter systems, such as polymeric systems [1–6] and amphiphilic systems [7–14].

Amphiphilic molecules, such as lipids and surfactants, contain hydrophilic and hydrophobic parts. In aqueous solvents, these molecules often spontaneously self-assemble into various structures, such as micelles, bilayer membranes, and bicontinuous structures [15–17]. The shape transitions of the micelles play an important role in cellular physiology and micellar drug delivery systems [18]. The transformation of micellar shapes has recently been investigated by coarse-grained molecular simulations [19–21]. Although numerous computer simulation studies have been carried out on micellar systems in amphiphilic solutions to date [22–25], the detailed mechanisms of micellar shape transition in amphiphilic solutions have not been fully understood at the molecular level.

This study aims to clarify the molecular mechanisms of micellar shape transitions in amphiphilic solutions. Our particular concern is to investigate the effect of hydrophilicity on the micellar shapes in amphiphilic solutions. The curvature of the tail-solvent interface in micelles tends to increase with increasing intensity of the hydrophilic interaction, which leads to the micellar shape change [9]. To investigate this at the molecular level, we performed molecular dynamics (MD) simulations of coarse-grained rigid amphiphilic molecules with explicit solvent molecules and systematically analyzed the micellar shape transitions.

2. Simulation Model and Method

The computational model is the same as that used in previous works [7–9, 13, 14]. An amphiphilic molecule is a rigid rod that is composed of one hydrophilic particle and two hydrophobic particles. The solvent molecules are modeled as hydrophilic particles. The interaction between hydrophilic and hydrophobic particles is modeled by the repulsive soft core potential given by Eq.(1)

$$U_{\rm SC}(r) = 4\varepsilon_{\rm SC}\left(\frac{\sigma_{\rm SC}}{r}\right)^9, \tag{1}$$

where r is the interparticle distance and $\varepsilon_{\rm SC}$ is an interaction parameter for the intensity of the hydrophobic interaction. The interaction between a hydrophilic head particle and a solvent particle is modeled by the Lennard-Jones (LJ) potential given by Eq.(2)

$$U_{\rm LJ-hs}(r) = 4\varepsilon_{\rm hs}\left[\left(\frac{\sigma}{r}\right)^{12} - \left(\frac{\sigma}{r}\right)^6\right]. \tag{2}$$
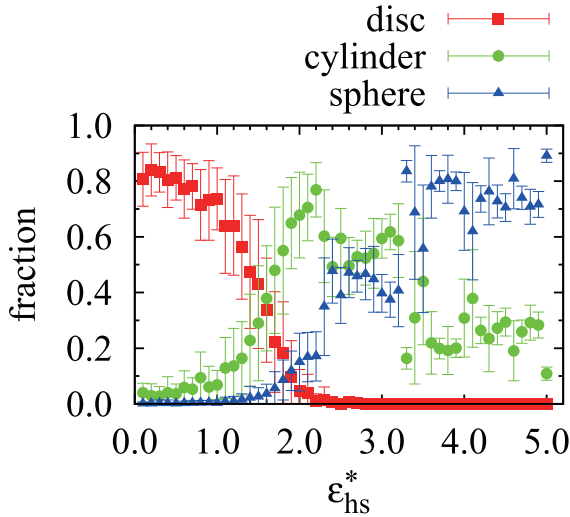
Fig. 1 The fraction of various micellar shapes versus the hydrophilic interaction parameter ε_{hs}^*.

All other interactions are modeled by the LJ potential given by Eq.(3)

$$U_{LJ}(r) = 4\varepsilon\left[\left(\frac{\sigma}{r}\right)^{12} - \left(\frac{\sigma}{r}\right)^6\right], \quad (3)$$

where ε_{hs} is an interaction parameter for the intensity of the hydrophilic interaction. The parameter σ_{SC} is set at $\sigma_{SC} = 1.05\sigma$ as in Ref. [22]. To avoid discontinuities in the potential energy and the force owing to the potential energy cutoff, we use the shifted force variant of these nonbonded potentials as given by Eq.(4)

$$V_X(r) = U_X(r) - U_X(r_c) - \left.\frac{\partial U_X}{\partial r}\right|_{r=r_c} (r - r_c), \quad (4)$$

where $X = SC$, LJ-hs or LJ and r_c is the cutoff distance, which is set at $r_c = 3.0\sigma$. In the following discussion, we denote dimensionless quantities with an asterisk, e.g., time $t^* = t\sqrt{\varepsilon/m\sigma^2}$ and temperature $T^* = k_B T/\varepsilon$, where k_B is the Boltzmann constant.

The equations of motion for all particles are numerically solved by using the leap-frog algorithm at constant temperature with a time step of $\Delta t^* = 0.0025$ and the temperature is controlled at every 10 time steps by *ad hoc* velocity scaling [26]. We apply periodic boundary conditions and the number density ρ^* is set at $\rho^* = 0.75$.

Initially, we prepare an isolated micelle of 97 amphiphilic molecules with $(\varepsilon_{SC}^*, \varepsilon_{hs}^*)=(1.0, 1.0)$ in solution at $T^* = 1.3$. The number of solvent particles is 5541, which leads to the amphiphilic concentration of 0.05. The intensity of the hydrophilic interaction ε_{hs}^* is then varied ($\varepsilon_{hs}^* = 0.1, 0.2, ..., 0.9, 1.1, 1.2, ..., 5.0$) and MD simulations of $t^* = 2.0 \times 10^4$ (8.0×10^6 time steps) are carried out for each simulation run.
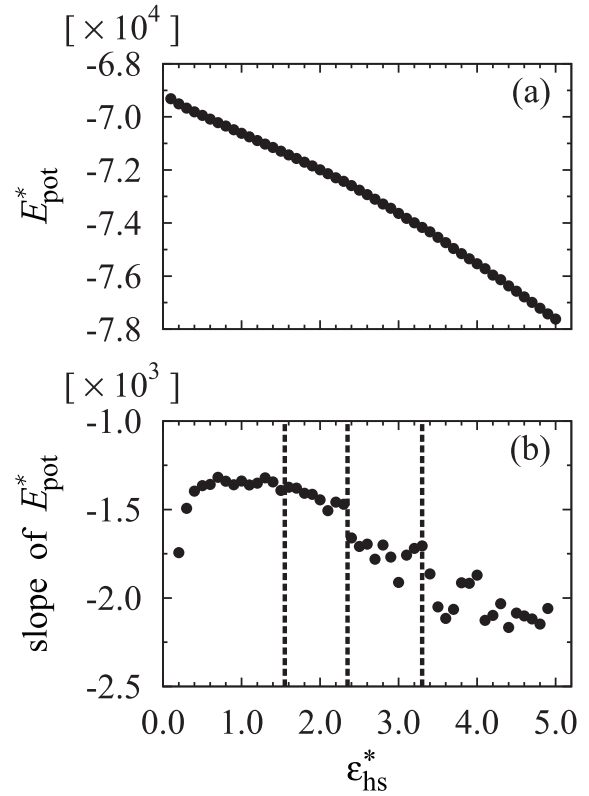
Fig. 2 (a) The total potential energy E_{pot}^* and (b) the slope of E_{pot}^* versus the hydrophilic interaction parameter ε_{hs}^*.

3. Simulation Results and Discussion
3.1 Fraction of micellar shapes

The dominant micellar shape changes from disc to cylinder and then to sphere as the intensity of the hydrophilic interaction ε_{hs}^* increases [8, 9, 13, 14]. We examined the micellar shape distribution to quantify how the micellar shape changes with hydrophilicity. Following previous studies [8, 9, 13, 14], we use the orientational order parameters as indices to characterize the micellar shapes. We introduce a coordinate system that consists of three principal axes of inertia of the micelle. The origin is located at the center-of-mass position of the micelle, the x-axis is the principal axis with the largest moment of inertia, and the z-axis is the principal axis with the smallest moment of inertia. The orientational order parameters p_x, p_y, and p_z are defined as follows:

$$p_i = \left\langle \frac{3\cos^2\theta_i - 1}{2} \right\rangle \quad (i = x, y, z), \quad (5)$$

where θ_i is the angle between the end-to-end vector of an amphiphilic molecule and the i-axis ($i = x, y, z$), and $\langle \cdots \rangle$ denotes the average over all amphiphilic molecules. The average for the amphiphilic molecules is taken near the center-of-mass position of the micelle; that is, in the region $-\Delta r < x, y, z < \Delta r$. We set $\Delta r = 2.5\sigma$ to calculate p_i. Ideally, the orientational order parameters take the following values: $(p_x, p_y, p_z) = (1, -0.5, -0.5)$ for disc, $(p_x, p_y, p_z) = (0, 0, -0.5)$ for cylinder and $(p_x, p_y, p_z) = (0, 0, 0)$ for

(a)

$t^* = 15000$ $t^* = 17000$

(b)

others
disc
cylinder
sphere

fraction

time t^* $[\times 10^3]$

(a)

$t^* = 19000$ $t^* = 20000$

(b)

others
disc
cylinder
sphere

fraction

time t^* $[\times 10^3]$
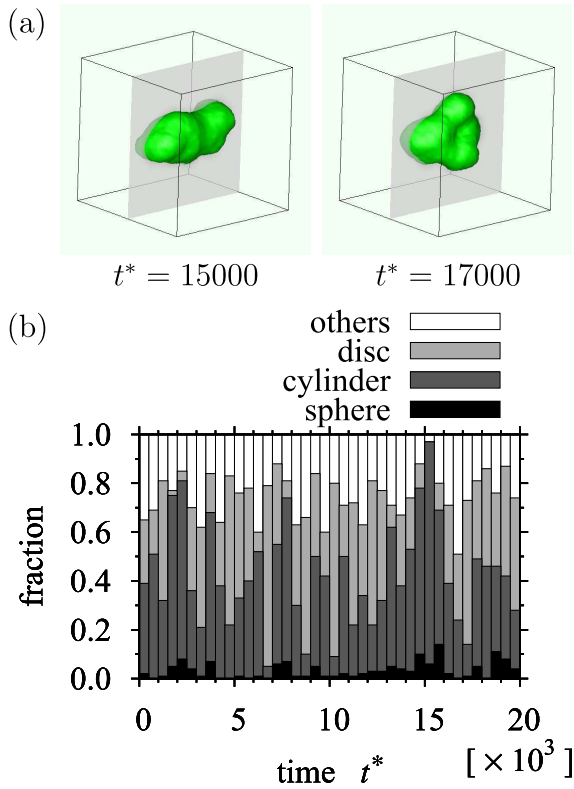
Fig. 3 (a) Snapshots of micelles formed by amphiphilic molecules at $t^* = 15000$ (cylindrical micelle) and $t^* = 17000$ (disc-shaped micelle) and (b) the time evolution of the fraction of various micellar shapes in the case of sudden increase of ε_{hs}^* from 1.0 to 1.6. In (a), isosurfaces of the density of the tail particles, which are calculated by Gaussian splatting techniques, are depicted to show the micellar shape clearly.

Fig. 4 (a) Snapshots of micelles formed by amphiphilic molecules at $t^* = 19000$ (cylindrical and spherical micelles) and $t^* = 20000$ (spherical micelles) and (b) the time evolution of the fraction of various micellar shapes in the case of sudden increase of ε_{hs}^* from 1.0 to 2.7. In (a), isosurfaces of the density of the tail particles, which are calculated by Gaussian splatting techniques, are depicted to show the micellar shape clearly.

sphere. Detailed analysis of the distribution functions of these orientational order parameters showed that, in practice, three types of micellar shapes are clearly distinguishable by the orientational order parameters: $0.5 < p_x < 1.0$ and $-0.5 < p_y, p_z < -0.25$ for a disc micelle, $-0.25 < p_x, p_y < 0.5$ and $-0.5 < p_z < -0.25$ for a cylindrical micelle, and $-0.25 < p_x, p_y, p_z < 0.5$ for a spherical micelle [8,9,13,14]. We calculate the fractions of the micellar shapes based on the orientational order parameters.

In Fig. 1, the fraction of various micellar shapes is shown as a function of the intensity of the hydrophilic interaction ε_{hs}^*. This figure shows that the dominant micellar shape is disc for $\varepsilon_{hs}^* < 1.6$, cylinder for $1.6 < \varepsilon_{hs}^* \leq 2.2$, and sphere for $\varepsilon_{hs}^* \geq 3.3$. It is also found that there exists a wide coexistence region in the intensity of the hydrophilic interaction between the cylinder and the sphere for $2.3 \leq \varepsilon_{hs}^* \leq 3.2$. There exists, on the other hand, a narrow coexistence region between the cylinder and the disc, which is located around $\varepsilon_{hs}^* \approx 1.6$. The micellar shapes are clearly distinguishable even in the coexistence region; that is, two kinds of micellar shapes (cylinder and sphere, or cylinder and disc) coexist dynamically.

3.2 Potential energy

Figure 2 shows the total potential energy E_{pot}^* and its slope as a function of the intensity of the hydrophilic interaction ε_{hs}^*. From this figure, we find the following characteristic features: (i) The total potential energy decreases monotonically even during the micellar shape transition as the intensity of the hydrophilic interaction increases and (ii) as the intensity of the hydrophilic interaction increases, the slope of the total potential energy decreases stepwise in relation to the micellar shape transition. It is noteworthy that the slope of E_{pot}^* stays nearly constant in the coexistence region of cylinder and sphere ($2.3 \leq \varepsilon_{hs}^* \leq 3.2$).

3.3 Dynamic coexistence of micellar shapes

We studied the dynamic coexistence of a cylindrical micelle and a disc-shaped micelle, observed at $\varepsilon_{hs}^* = 1.6$ (Fig. 3), and that of a cylindrical micelle and a spherical micelle, observed at $\varepsilon_{hs}^* = 2.7$ (Fig. 4). In Fig. 3, we show the snapshots of micelles and the time dependence of the fraction of the various micellar shapes at $\varepsilon_{hs}^* = 1.6$. Isosurfaces of the density of the tail particles, which are shown in Figs. 3 (a) and 4 (a) to clarify the micellar shapes, are

calculated by Gaussian splatting techniques. The Gaussian splatting techniques build topological structures by sampling unstructured points into an image dataset with a Gaussian splatting function [27]. Figure 3 shows that the dominant micellar shape alternates between cylinder and disc. Figure 4 shows the snapshots of micelles and the time dependence of the fraction of the various micellar shapes at $\varepsilon_{hs}^* = 2.7$. This figure suggests that although the individual micellar shapes alternate between a cylinder and a sphere, the distribution of the fraction of the various micellar shapes as a whole remains nearly constant over time.

4. Conclusions

We have carried out MD simulations of coarse-grained rigid amphiphilic molecules with explicit solvent molecules. By analyzing the microscopic processes of micellar shape transition, the following conclusions were reached: (1) As the intensity of the hydrophilic interaction ε_{hs}^* increases, the dominant micellar shape changes from disc to cylinder and then to sphere. (2) The potential energy decreases monotonically even during the shape transition of micelles as ε_{hs}^* increases. (3) As the hydrophilic interaction increases, the slope of the potential energy decreases stepwise in relation to the micellar shape transition. (4) The slope of the potential energy stays roughly constant in the coexistence region between cylinder and sphere. (5) Finally, there exists a wide coexistence region in the intensity of the hydrophilic interaction between cylinder and sphere, whereas the coexistence region between cylinder and disc is very narrow.

The fourth observation is not necessarily obvious. At the present stage, we cannot propose a physical explanation for the constancy of the slope of E_{pot}^*. To elucidate this, an elaborate energy analysis must be performed, which is the subject of future work.

In the future, we will also carry out MD simulations of larger systems to investigate the effect of the intermicellar interaction on the transition process of micellar shapes in detail.

Acknowledgment

[1] S. Fujiwara and T. Sato, J. Chem. Phys. **107**, 613 (1997).
[2] S. Fujiwara and T. Sato, J. Chem. Phys. **114**, 6455 (2001).
[3] S. Fujiwara and T. Sato, Phys. Rev. Lett. **80**, 991 (1998).
[4] S. Fujiwara and T. Sato, J. Chem. Phys. **110**, 9757 (1999).
[5] S. Fujiwara and T. Sato, Comput. Phys. Commun. **142**, 123 (2001).
[6] S. Fujiwara, M. Hashimoto, T. Itoh and H. Nakamura, J. Phys. Soc. Jpn. **75**, 024605 (2006).
[7] S. Fujiwara, M. Hashimoto and T. Itoh, J. Plasma Phys. **72**, 1011 (2006).
[8] S. Fujiwara, T. Itoh, M. Hashimoto and Y. Tamura, Mol. Simul. **33**, 115 (2007).
[9] S. Fujiwara, T. Itoh, M. Hashimoto and R. Horiuchi, J. Chem. Phys. **130**, 144901 (2009).
[10] S. Fujiwara, T. Itoh, M. Hashimoto, H. Nakamura and Y. Tamura, Plasma Fusion Res. **5**, S2114 (2010).
[11] S. Fujiwara, D. Funaoka, T. Itoh and M. Hashimoto, Comput. Phys. Commun. **182**, 192 (2011).
[12] S. Fujiwara, T. Itoh, M. Hashimoto, Y. Tamura, H. Nakamura and R. Horiuchi, Plasma Fusion Res. **6**, 2401040 (2011).
[13] S. Fujiwara, M. Hashimoto, T. Itoh and R. Horiuchi, Chem. Lett. **41**, 1038 (2012).
[14] S. Fujiwara, M. Hashimoto, T. Itoh, H. Nakamura and Y. Tamura, J. Phys.: Conf. Ser. **454**, 012024 (2013).
[15] J.N. Israelachvili, *Intermolecular and Surface Forces* (Academic Press, London, 1992) 2nd ed.
[16] *Micelles, Membranes, Microemulsions, and Monolayers*, edited by W.M. Gelbart, A. Ben-Shaul and D. Roux (Springer-Verlag, New York, 1994) pp.1–104.
[17] I.W. Hamley, *Introduction to Soft Matter* (J. Wiley, Chichester, 2007) Rev. ed.
[18] A. Chaudhuri, S. Haldar and A. Chattopadhyay, Chem. Phys. Lipids **165**, 497 (2012).
[19] A.V. Sangwai and R. Sureshkumar, Langmuir **27**, 6628 (2011).
[20] M. Velinova, D. Sengupta, A.V. Tadjer and S.J. Marrink, Langmuir **27**, 14071 (2011).
[21] A.G. Daful, J.B. Avalos and A.D. Mackie, Langmuir **28**, 3730 (2012).
[22] R. Goetz and R. Lipowsky, J. Chem. Phys. **108**, 7397 (1998).
[23] R. Goetz, G. Gompper and R. Lipowsky, Phys. Rev. Lett. **82**, 221 (1998).
[24] S.J. Marrink, D.P. Tieleman and A.E. Mark, J. Phys. Chem. B **104**, 12165 (2000).
[25] E.N. Brodskaya, Colloid J. **74**, 154 (2012).
[26] M.P. Allen and D.J. Tildesley, *Computer Simulation of Liquids* (Clarendon, Oxford, 1987).
[27] W. Schroeder, K. Martin and B. Lorensen, *The Visualization Toolkit: An Object-Oriented Approach to 3D Graphics* (Kitware, New York, 2002) 3rd ed.